Identification of the Allosteric Regulatory Site in Bacterial Phosphoribulokinase†

Guosheng Kung, Jennifer A. Runquist, Henry M. Miziorko, and David H. T. Harrison*

Department of Biochemistry, Medical College of Wisconsin, Milwaukee, Wisconsin 53226

Received May 5, 1999; Revised Manuscript Received August 13, 1999

ABSTRACT: Bacterial phosphoribulokinases (PRKs) are octameric members of the adenylate kinase family of enzymes. The enzyme is allosterically activated by NADH and allosterically inhibited by AMP. We have determined the crystal structure of PRK from *Rhodobacter sphaeroides* bound to the ATP analogue AMP-PCP to a resolution of 2.6 Å. The structure reveals that the ATP analogue does not bind to the canonical ATP site found in adenylate kinase family members. Rather, the AMP-PCP binds in two different orientations at the interface of three of the monomers in the octamer. This interface was previously characterized as having an unusually large number of arginine residues. Of the five arginine residues that are near the bound nucleotide, one (Arg 221) is highly conserved in both prokaryotic and eukaryotic (nonallosterically regulated) PRKs, two (Arg 234 and Arg 257) are on a second subunit and conserved in only prokaryotic PRKs, and two (Arg 30 and Arg 31) are on a third subunit with only one of them (Arg 31) conserved in prokaryotic PRKs. Each of these arginine residues was converted by site-directed mutagenesis to alanine. Fluorescence binding data suggest that none of these arginines are involved in active site ATP binding and that Arg 234 and Arg 257 on the second subunit are directly involved in NADH binding, while the other arginines have a minimal effect on NADH binding. While the wild-type enzyme exhibits low maximal activity and hyperbolic kinetics with respect to ATP in the absence of NADH and high maximal activity and sigmoidal kinetics in the presence of NADH, the R31A mutant exhibits identical hyperbolic kinetics with respect to ATP in the presence or absence of NADH. Thus, the transmission of allosteric information from one subunit to another is conducted through a single path that includes NADH and Arg 31.

The synthesis of ribulose 1,5-bisphosphate (RuBP) by PRK (EC 2.7.1.19) is essential for the creation of all new biomass (e.g., sugars, proteins, and lipids) in the biosphere. PRK catalyzes an in-line phosphoryl transfer (*1*) from magnesium adenosine triphosphate (Mg•ATP) to ribulose 5-phosphate (Ru5P) to form magnesium adenosine diphosphate (Mg•ADP) and ribulose 1,5-bisphosphate (RuBP), the CO_2 acceptor in Calvin's reductive pentose phosphate cycle. The quaternary structures and regulatory properties of PRK from different organisms can be divided along prokaryotic and eukaryotic lines. Most prokaryotic PRKs exist as octamers of 32 kDa subunits (*2*) and are subject to allosteric regulation (*3*). Eukaryotic PRKs are dimers of about 40 kDa and are regulated by reversible oxidation and reduction of cysteine sulfhydryls (*4*). Recently, it has been shown that eukaryotic PRKs are also regulated by forming complexes with other "Calvin cycle" enzymes (*5*).

Allosteric activation and inhibition are common regulatory mechanisms involved in nearly every metabolic and signal transduction pathway. Unlike the other allosterically regulated enzymes for which atomic resolution structures are available [e.g., ATCase (*6*, *7*) and glycogen phosphorylase (*8*)], PRK from *Rhodobacter sphaeroides* is a member of a class of enzymes which exhibit Michaelis−Menten kinetics in the absence of allosteric regulators and sigmoidal kinetics in the presence of the allosteric regulator NADH. Adenine-containing mono- and dinucleotides can bind at the effector site (NADH activates and AMP inhibits PRK). Occupancy of the *Alcaligenes eutrophus* PRK effector site by nucleotide is unaffected by substrate ATP (*2*), indicating physically distinct effector and catalytic sites. The substrate ATP site on PRK has been assigned, in part, on the basis of the consensus that has developed for NMP kinase fold enzymes. For PRK, this substrate site is formed by the edge of a β-sheet region which includes a Walker B sequence and is flanked by a "P-loop" or Walker A motif. Additionally, mutagenesis work has identified essential residues such as D42 in this region as well as K165 or D169 in the helical "lid" that represents the opposing boundary of the catalytic site.

Additionally, PRK is the first member of the nucleotide monophosphate kinase structural family to be studied that exhibits allosteric kinetics. To understand the structural basis for allosteric regulation, we have determined the three-dimensional structure of PRK from *R. sphaeroides* bound to the ATP analogue AMP-PCP. The ATP analogue is not bound at the canonical phosphoryl donor site of the nucleotide monophosphate kinase family, but to a site at the interface between three subunits. To verify the authenticity of this proposed allosteric site, we have mutated five arginine residues and characterized these mutant enzymes for their

† This work was supported by a Herman-Frasch Award to D.H.T.H. and by a grant from the U.S. Department of Agriculture (NRI-CGP) to H.M.M.

* To whom correspondence should be addressed: Department of Biochemistry, Medical College of Wisconsin, 8701 Watertown Plank Rd., Milwaukee, WI 53226. Phone: (414) 456-4432. Fax: (414) 456-6510.

10.1021/bi991033y CCC: $18.00
Published on Web 10/29/1999

Table 1: Primers for Site-Directed Mutagenesis[a]

mutant	up primer	down primer
R30A	5′gccttgacccccctcgcgc**gc**gaagatctggtcg3′	5′cgaccagatcttc**gc**gcgcgagggggtcaaggc3′
R31A	5′gccttgacccccctcg**gc**ccgcgaagatctggtcg3′	5′cgaccagatcttccg**gc**cgagggggtcaaggc3′
R221A	5′tggggatccag**gc**cgcgatgaag3′	5′cttcatcgcg**gc**ctggatcccca3′
R234A	5′gcgcggattgcggaaa**gc**gatcaccaccacgc3′	5′gcgtggtggtgatc**gc**tttccgcaatccgcgc3′
R257A	5′caggatggaattggcg**gc**gctcatccacgagcc3′	5′ggctcgtggatgagc**gc**cgccaattccatcctg3′

[a] To amplify the left and right arms of the bacterial *prkA* gene in the pETbprkwt plasmid, the up primer was used with the T7 primer and the down primer was used with the T7 terminator primer.

Table 2: Crystallographic Refinement Data for AMP-PCP Bound to PRK[a]

	working				free			
resolution range (Å)	no. of reflections	completeness (%)	shell *R*-factor	accum *R*-factor	no. of reflections	completeness (%)	shell *R*-factor	accum *R*-factor
5.14−15	1427	87.1	0.202	0.202	91	5.5	0.309	0.309
4.11−5.14	1358	88.8	0.160	0.182	58	3.9	0.281	0.299
3.60−4.11	1318	88.2	0.190	0.184	72	4.6	0.264	0.290
3.27−3.60	1304	88.5	0.226	0.191	69	4.6	0.279	0.288
3.04−3.27	1277	88.5	0.267	0.200	60	4.3	0.316	0.290
2.86−3.04	1247	86.4	0.284	0.207	51	3.3	0.321	0.293
2.72−2.86	1196	83.6	0.298	0.213	73	5.1	0.322	0.295
2.60−2.72	1175	81.8	0.334	0.222	58	3.9	0.408	0.301
2.60−15	10302	86.6		0.222	535	4.4		0.301
deviation from ideality					Ramachandran plot (%)			
bond lengths (Å)			0.010		most favored		88.5	
bond angles (deg)			1.22		additionally allowed		10.2	
					others		1.3	

[a] *R*-factor and bond ideality statistics were computed with XPLOR (*14*), and Ramachandran statistics were computed using PROCHECK (22).

ability to bind the allosteric effector NADH or the fluorescent ATP analogue TNP-ATP. While NADH only binds to the allosteric site, the fluorescent ATP analogue is known to bind only at the active site. Further, we have characterized the kinetics and allosteric properties of each mutant enzyme.

MATERIALS AND METHODS

Materials. Deoxyoligonucleotides and fluorescein-labeled sequencing primers were purchased from Operon Technologies, Inc. T4 DNA ligase was purchased from New England Biolabs. Restriction enzymes were obtained from Promega. *Pfu* DNA polymerase was purchased from Stratagene. AMP-PCP was a product of Sigma. Plasmid pET3d was from Novagen. Isolation of plasmid DNA grown in *Escherichia coli* JM105 cells was accomplished using Qiagen's Plasmid Mini and Midi Kits. Isolation of DNA fragments was accomplished using a QIAEX II Gel Extraction Kit. DNA sequence analysis was performed using a Pharmacia/LKB ALF DNA sequencer. For recombinant protein expression, ampicillin was purchased from Fisher Scientific and isopropyl β-D-thiogalactoside (IPTG) from Research Products International Corp. Adenosine 5′-triphosphate, DTT, β-NADH, D-ribulose 5-phosphate, 2-mercaptoethanol, and Tris buffer were obtained from Sigma Chemical Co., and Hepes buffer was obtained from Research Organics, Inc. Sodium [^{14}C]-bicarbonate (56 mCi/mmol) was a product of American Radiolabeled Chemicals, Inc. Chromatography media utilized for the isolation of PRK and PRK mutants included reactive green-19 agarose from Sigma Chemical Co. and Q Sepharose Fast Flow from Pharmacia Biotech. TNP-ATP [2′(3′)-*O*-(2,4,6-trinitrophenyl)adenosine 5′-triphosphate] was purchased from Molecular Probes. The RuBP carboxylase required for the CO_2 fixation assay of PRK activity was isolated after expression in *E. coli* JM103 cells using a plasmid generously provided by C. R. Somerville.

Construction of prkA Mutant Alleles. The mutant alleles of prkA encoding the single-amino acid substitutions R30A, R31A, R221A, R234A, and R257A were constructed using pETbprkwt. Construction of these mutants was accomplished using the PCR overlap-extension technique. For each mutation, two overlapping primers were commercially synthesized by Life Technologies; the sequences of the primers are listed in Table 1. Site-directed mutagenesis was performed using the T7 primer and the mutagenic up-primer, or the mutagenic down-primer and the T7 terminator primer to amplify the left and right arms of each mutant using pETbprkwt as the template. The T7 primer and T7 terminator primer were used to amplify the full-length *prkA* mutant using the left and the right arms as the template. PCR was carried out using the high-fidelity DNA enzyme *pfu* DNA polymerase (Stratagene). The PCR products were cut with *Nco*I (Promega) and were ligated to pET-3d digested with *Nco*I. The orientation and the sequences of the inserts were confirmed using a Pharmacia DNA sequencing kit and the Pharmacia/LKB ALF DNA sequencer.

Expression and Purification of PRK. E. coli BL21(DE3) cultures containing plasmids pETbprkR30A, pETbprkR31A, pETbprkR221A, pETbprkR234A, and pETbprkR257A were grown at 25 °C in 1 L of ampicillin-containing LB medium to an OD_{600} of 0.6. Expression of the PRK mutants was induced by addition of IPTG to a final concentration of 1 mM followed by additional growth for 3−4 h. The cells were collected by low-speed centrifugation; cell pellets were suspended and disrupted using a French pressure cell. A 100000*g* supernatant was prepared and subjected to Q-Sepharose anion exchange chromatography followed by affinity chromatography on reactive green-19 agarose. PRK

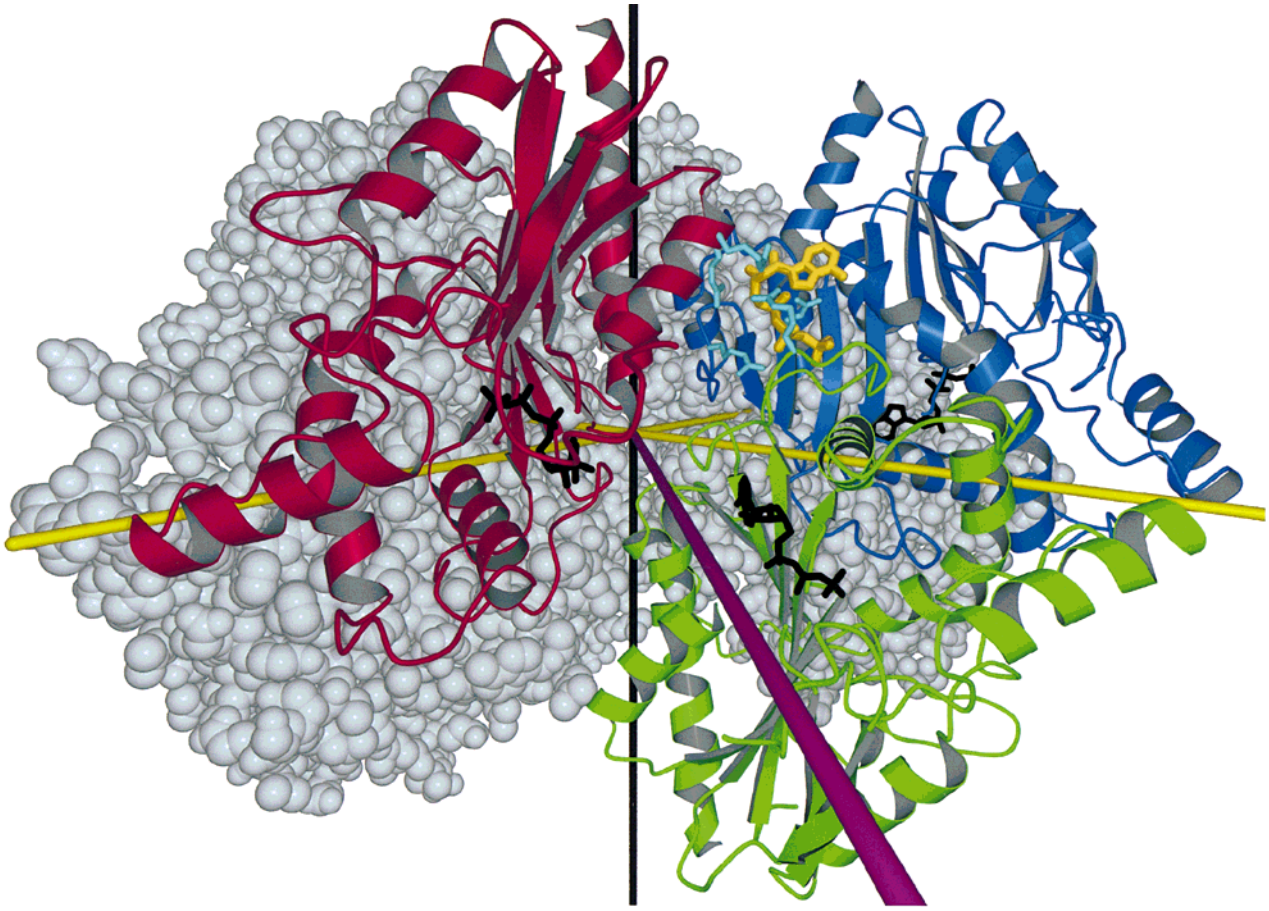

FIGURE 1: Location of one of eight AMP-PCP binding sites on the PRK octamer. The vertical black axis is the 4-fold symmetry axis, and the yellow and magenta axes are 2-fold symmetry axes. The three subunits (blue, green, and red) shown as ribbon models each make contact with the AMP-PCP molecule. The arginines that were mutated are light blue, and the AMP-PCP is gold. In black are modeled in ATP molecules that show the active site region of PRK. The active site of the green subunit faces the active site of the red subunit, and the two subunits are related by a 2-fold symmetry axis that runs through the octamer (the magenta axis). The green subunit and the blue subunit have their active sites facing away from each other, and these two subunits are related by a different 2-fold symmetry axis (the yellow axis). The green and blue subunits alone are thought to be a model of the eukaryotic dimeric PRK.

was eluted from reactive green-19 agarose affinity resin with a buffer containing 25 mM Tris-HCl (pH 8.2), 10 mM 2-mercaptoethanol, 1 mM EDTA, and 10 mM ATP. ATP removal from the ATP-eluted enzyme was accomplished by prolonged dialysis. For quantitative protein concentration estimates, an extinction coefficient of 50 303 M^{-1} cm^{-1} at 280 nm was used (*9*). The protein concentration was also determined by the method of Bradford (*10*) using bovine serum albumin as a standard with an appropriate correction.

TNP-ATP Stoichiometry Measurements. TNP-ATP binding to PRK and PRK mutants was followed by fluorescence measurements utilizing a SLM 4800C spectrofluorometer as described previously (*9*). For data analysis, values measured at the fluorescence emission peak of 545 nm for PRK-bound TNP-ATP were ascertained. The stoichiometry of binding of this mononucleotide to PRK and PRK mutants was determined from the intersection point of lines fit to the low-occupancy and plateau regions of the titration data by linear regression. Calculated stoichiometries reflect the number of binding sites per 32 kDa PRK or PRK mutant.

NADH Binding. NADH binding to PRK and PRK mutants was also assessed using fluorescence methods as described previously (*9*). For data analysis, values measured at the fluorescence emission peak of 440 nm for PRK-bound NADH were obtained. Fluorescence due to free NADH is subtracted from the data points to ascertain the fluorescence enhancement due to ligand binding. The data points were fit to a single-site ligand binding equation using nonlinear regression (*11*). The equation is $y = [L]Cap/(K_d + [L])$, where y is the fluorescence enhancement measured for PRK-bound NADH and Cap is the maximum fluorescence enhancement generated by bound ligand. The dissociation constant for dissociation of the ligand from the binding site is K_d. [L] is the ligand concentration.

Kinetic Characterization of PRK. A radioisotopic assay that involves trapping the PRK reaction product RuBP via the RuBP carboxylase-dependent incorporation of $^{14}CO_2$ to form acid-stable [^{14}C]-3-phosphoglycerate (*12*) was utilized. In standard assays, the final concentrations of reaction mixture components were 100 mM Hepes (pH 8.0), 1 mM DTT, 20 mM $MgCl_2$, 20 mM $KH^{14}CO_3$ (1000 dpm/nmol), 5 mM ATP, 1 mM Ru5P, 1 mM NADH, and 100 milliunits of recombinant RuBP carboxylase. Enzyme assays were conducted at 30 °C. For kinetic characterization of the mutant proteins, ATP concentration ranges varied from 0.05 to 15 mM; Ru5P concentration ranges varied from 0.05 to 8 mM. Kinetic data were fit by a nonlinear regression analysis algorithm (*11*).

Crystallization and X-ray Data Collection. Native crystals of PRK were obtained as described by Harrison et al. (*13*)

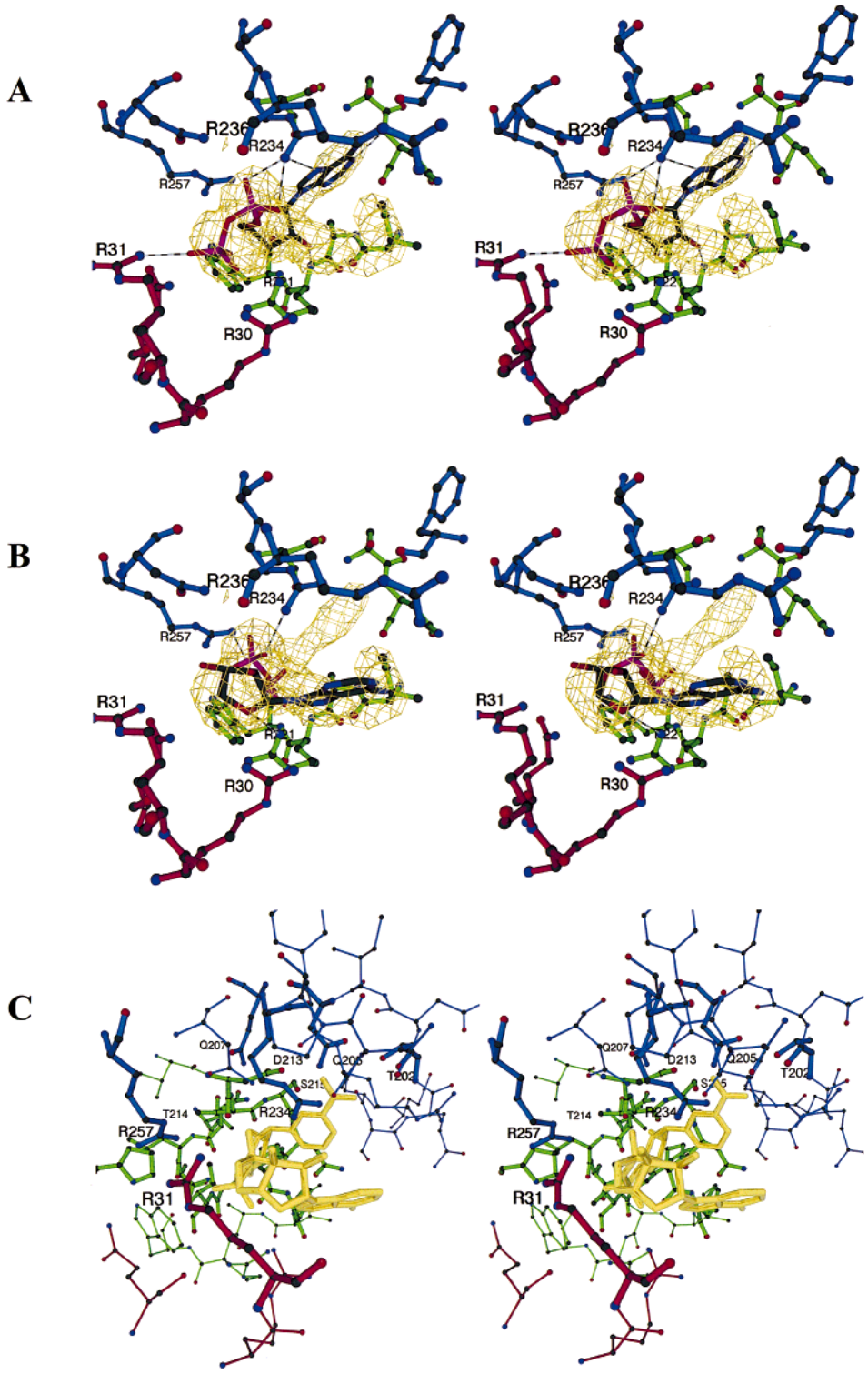

FIGURE 2: (A) Initial difference electron density map with the lower-temperature factor AMP-PCP orientation. Refined model of PRK (ball and stick with CPK; colored balls and blue, green, and red sticks for each subunit) and AMP-PCP (half-bonds with CPK; carbon, black; nitrogen, blue; oxygen, red; phosphorus, magenta) placed in electron density (gold) contoured at 3σ above background. The difference electron density map ($F_{obs} - F_{calc}$ as Fourier coefficients) was calculated using the apo-PRK structure as a model (IA7J) for generating calculated structure factors and phases. (B) Initial difference electron density map with the higher-temperature factor AMP-PCP orientation. (C) Model of NADH bound to the allosteric site of PRK. This model is based on a combination of the two AMP-PCP orientations, where the ADP ribose is placed to closely match the higher-temperature factor AMP-PCP molecule, and the nicotinamide is placed in a manner similar to that of the lower-temperature factor orientation with adjustments to the model to avoid steric conflicts. Residues that are conserved only in bacterial species of PRK are depicted as thick ball-and-stick representations, whereas other residues are depicted as thin ball-and-stick representations. The NADH is shown as a gold stick model. In addition to the model that is shown, it is possible to place the nicotinamide in the pocket near Thr 214; however, the model that is presented more faithfully mimics the AMP-PCP structure. Since there is likely to be substantial changes in the conformation of this site upon NADH binding, the value of the model is to suggest residues that may be important to NADH binding.

Table 3: Binding Parameters for Binding of Ligands to PRK Mutant Enzymes

enzyme	$n_{TNP-ATP}$[a]	K_{dNADH}[b] (μM)	K_{aNADH}[c] (μM)
wild-type	0.84 ± 0.03	2.60 ± 0.55	101 ± 19.5
R30A	0.90 ± 0.08	10.90 ± 2.27	67.3 ± 20.2
R31A	0.67 ± 0.10	26.00 ± 12.00	not detectable
R221A	0.83 ± 0.08	2.34 ± 0.54	NA
R234A	1.30 ± 0.08	not detectable	1800 ± 633
R257A	1.10 ± 0.10	not detectable	not detectable

[a] *n* denotes the calculated number of binding sites per subunit. Stoichiometries for TNP-ATP binding were determined from fluorescence titrations as described in Materials and Methods. See also Runquist et al. (*9*). [b] The data for K_{dNADH} were generated from fluorescence enhancement binding titrations. A nonlinear regression fit of the fluorescence data was performed using a hyperbolic saturation curve for binding of a single ligand to a protein (see Materials and Methods). [c] The data for the activation constant, K_{aNADH}, were generated from measuring the relative PRK activities at a series of NADH concentrations ranging from 0 to 10 mM using the radioactive CO_2 fixation assay (see Materials and Methods).

with $(NH_4)_2SO_4$ as the precipitant. Crystals of the complexes of PRK with AMP-PCP were prepared by cocrystallization of the native enzyme in the presence of 5 mM AMP-PCP, with 200 mM glycine, l00 mM Li_2SO_4, and 8% PEG8000. Additionally, the solution contained the additives 20 mM spermidine and 0.75% β-octyl glucoside. It was also possible to soak native PRK crystals in 50 mM Tris-HCl (pH 6.5), 15% PEG8000, 50 mM Li_2SO_4, and 5 mM AMP-PCP, which provided higher-resolution data. A single crystal (0.25 mm × 0.25 mm × 0.25 mm) of the "soaked in" complex was mounted in a 0.7 mm quartz capillary and irradiated with monochromated CuKα radiation from a Rigaku RU-200 X-ray generator using a 0.2 mm filament set to 50 kV and 100 mA. Diffraction data were collected on an R-axis imaging plate, and the images were processed with the HKL program suite. Crystals of the complex are isomorphous with respect to the native crystals and in space group *P*432, with an *a* of 130.1 Å. The overall *R*-merge for the data was 9% to 2.6 Å resolution.

Structure Determination and Refinement. As the crystal was isomorphous with respect to the unliganded crystal, difference Fourier methods were used to determine the structure of the complex. Crystallographic calculations were carried out with the X-PLOR program package (*14*), and model building was carried out with the program O (15). Initial phases were calculated from the coordinates of the refined, unliganded enzyme, which has a crystallographic *R*-factor of 21.3% at 2.5 Å resolution (*13*). Before any substrate modeling was done, rigid body and conventional positional refinement were performed. Difference electron density maps using either $2F_{obs} - F_{calc}$ or $F_{obs} - F_{calc}$ as Fourier coefficients were calculated from these coordinates. These maps were then used to model the AMP-PCP molecule. The electron density map allows the AMP-PCP molecule to be placed in two different orientations, each with 50% occupancy. Further, the terminal phosphoryl could not be placed in the electron density. During the course of refinement, both orientations of the AMP-PCP molecule were refined independently and these refinements gave consistently higher *R*-free values than when both orientations were refined. The *R*-free value converged after group temperature factors and nine low-temperature factor water molecules were added to the model. It was not possible to fit the P-loop region, residues 15−19, residues 100−108, or residues 173−175. The three residues that have poor Ramachandran statistics are Lys 3, Val 21, and Ala 171. These residues are near poorly ordered regions of the protein located at the amino terminus, near the P-loop, and near the flexible region between helices E and F. The details of the refinement statistics are given in Table 2.

RESULTS

Allosteric Site. The structure of PRK bound to AMP-PCP (an ATP analogue) was determined using the phases from the apoenzyme structure. A model of PRK bound to AMP-PCP in both of two orientations was refined as discussed in Materials and Methods. Unlike the ATP binding site of other members of the nucleotide monophosphate kinase family (*16*−*18*), this binding site is not located near the P-loop. Further, there is no indication of any substantial changes in protein conformation as a result of binding to the ATP analogue. Since the crystal is formed at pH 6.5, it is not surprising that the nucleotide does not bind to the active site since it has been shown not to do so at pH 5.5 in the binary complex (*9*). Rather, the octamer retains its 422 symmetry, and the AMP-PCP molecule is bound at the intersection of three protomers within the PRK octamer (Figure 1). As noted elsewhere, the octamer may be described as a tetramer of dimers, the dimers being conserved by evolution (*13*). In

Table 4: Steady State Kinetic Parameters for PRK and Its Mutants

enzyme	V_{max}[a] (units/mg)	$K_{m,Ru5P}$[b] (mM)	$S_{1/2-ATP}$[c] (mM)	Hill coefficient (ATP)	stimulation by NADH[d] (fold)
wild-type	338 ± 18	0.096 ± 0.014	0.55 ± 0.16	1.98 ± 0.15	30
wild-type without NADH	11.4 ± 1.3	0.062 ± 0.011	11.4 ± 0.94	hyperbolic	NA
R30A	154 ± 17	0.216 ± 0.074	3.62 ± 0.23	2.34 ± 0.45	40
R31A	12.6 ± 1.1	0.125 ± 0.017	8.81 ± 1.28	hyperbolic	1.1
R221A	52.4 ± 3.0	3.311 ± 0.336	5.00 ± 0.50	2.38 ± 0.59	>15
R234A	66.0 ± 5.1	0.122 ± 0.026	2.66 ± 0.19	1.86 ± 0.27	2.7
R257A	12.0 ± 0.5	0.381 ± 0.196	1.82 ± 0.12	1.64 ± 0.25	1.4
R186Q[e]	270 ± 13	0.048 ± 0.004	0.17 ± 0.02	hyperbolic	6.5

[a] The maximal velocity, given in micromoles per minute per milligram, is estimated from the Michaelis−Menten equation fit to the Ru5P saturation data. [b] $K_{m,Ru5P}$ is the ribulose 5-phosphate concentration at half-maximal velocity, as calculated from a nonlinear regression fit of the Ru5P saturation data to the Michaelis−Menten equation. [c] The $S_{1/2-ATP}$ is the ATP concentration at half-maximal velocity, as calculated from a fit of the ATP saturation data to the Hill equation. However, when the ATP saturation curve was hyperbolic rather than sigmoidal, the Michaelis−Menten equation was used to determine the $S_{1/2-ATP}$. [d] The stimulation is the maximal activation seen for the wild type and the mutants over the wide range of NADH concentrations that was employed (0, 0.1, 0.3, 0.5, 1, 5, and 10 mM). For the wild type, R30A, R31A, and R257A, the stimulation at 1.0 mM NADH was the same as the stimulation at 10 mM. Only for R234A did the level of NADH activation increase between 1 and 10 mM (K_{aNADH} of 1800 μM, Table 3). [e] Data published by Runquist et al. (*19*).

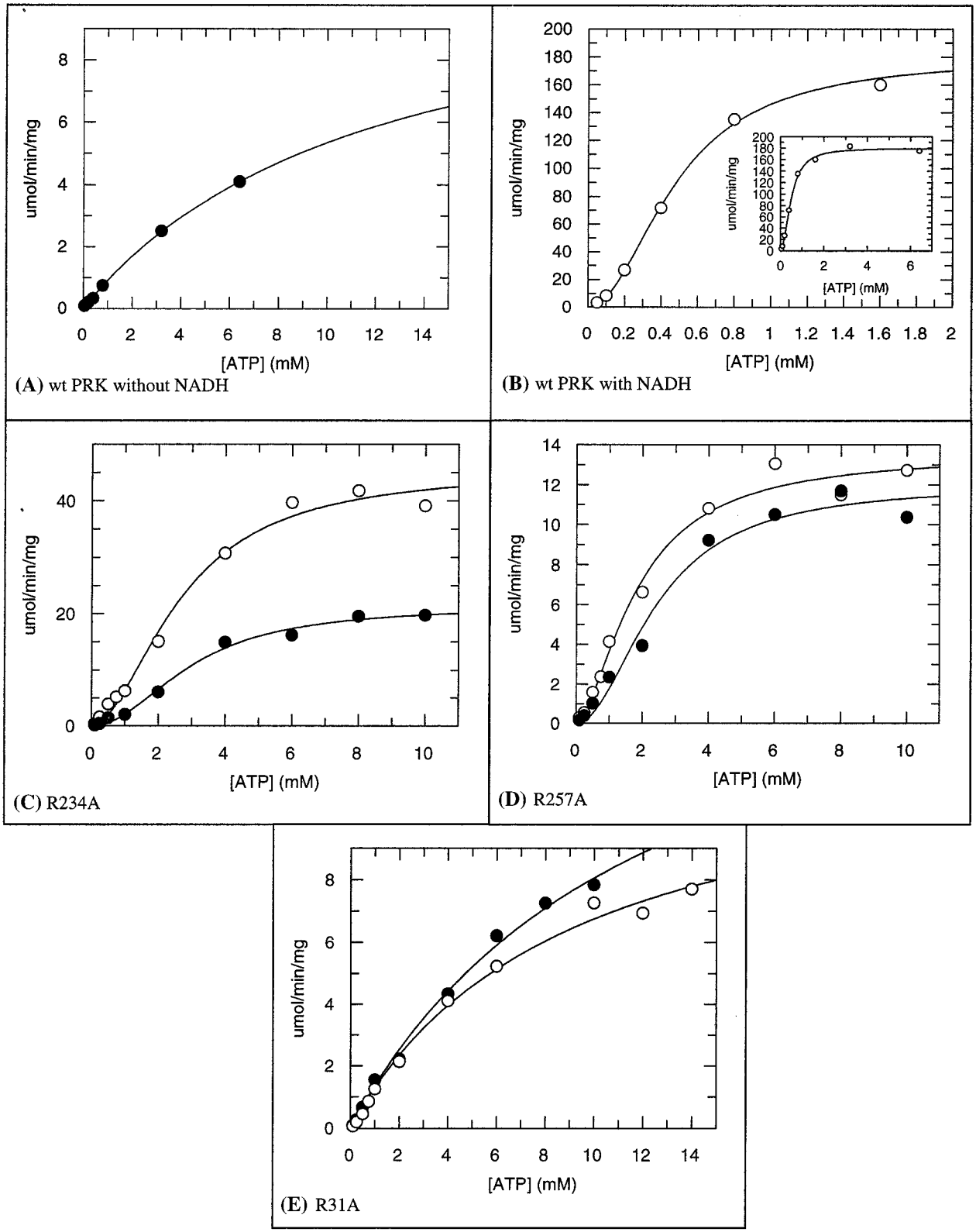

FIGURE 3: Reaction rate as a function of ATP concentration measured at 1 mM Ru5P. The white circles show the rate in the presence of 1 mM NADH, and the black circles show the rate in the absence of NADH. (A) The wild-type enzyme in the absence of NADH exhibits hyperbolic kinetics (*9*). (B) The wild-type enzyme in the presence of 1 mM NADH exhibits sigmoidal kinetics; the inset shows the extended concentration range. (C) The R234A mutant and (D) the R257A mutant enzymes exhibit sigmoidal kinetics in the presence or absence of NADH. (E) However, the R31A mutant enzyme exhibits hyperbolic kinetics in the presence or absence of NADH.

Figure 1, the blue and green protomer interface is conserved by evolution. The active sites within each dimer face away from each other and occupy a position in either the upper layer or the lower layer of the octamer. The major axis of an ellipsoid representing the dimer is tilted to form a right-handed pinwheel with respect to the tetramer's 4-fold axis of symmetry. The active site of a monomer from the upper layer faces (by 2-fold symmetry) the active site of a monomer

in the lower layer. In Figure 1, the active site of the red protomer faces the active site of the green protomer.

Both overlapping orientations of the AMP-PCP molecule are located at the edge of the conserved dimer interface and between two facing monomers from the upper and lower layers. A network of hydrogen bonds and salt bridges from the protein to the ribose and phosphoryl oxygens bind the nucleotide (Figure 2A,B). In the lower-temperature factor orientation (Figure 2A), N1 of the adenosine ring is 3.0 Å from the backbone amide nitrogen of Asn 216. O2′ of the ribose ring is 2.4 Å from the amide nitrogen of Arg 221 and 2.9 Å from the carbonyl oxygen of Ile 219. NH2 of Arg 234 is within hydrogen bonding distance of both nonbridging α-phosphate oxygens and N7 of the adenosine ring with distances of 2.4, 2.8, and 2.8 Å, respectively. One of the *β*-phosphoryl oxygens is 2.6 Å from NH2 of Arg 31. In the other "higher-temperature factor" orientation (Figure 2B), O2′ of the ribose ring is 2.8 Å from the carbonyl oxygen of Arg 236 (blue protomer). The ring O4′ is 2.7 Å from NH2 of Arg 30 (red protomer). NH1 of Arg 234 is 2.8 and 3.5 Å from the α-phosphoryl oxygens. Arg 257 is 3.4 Å from one of the *β*-phosphoryl oxygens.

On the basis of the structure of the bound high-temperature factor AMP-PCP, a model of NADH was built into this putative allosteric binding site (Figure 2C). The adenosine diphosphate moiety of the NADH is in the same location as that of the AMP-PCP. The nicotinamide-bearing ribose ring is placed in nearly the same location as the terminal phosphoryl, and the nicotinamide ring extends into the cleft. Torsion angles along the phosphoryl chain and the glycosidic bond were set to optimize hydrogen bonding and steric considerations. Examination of the kinetics and binding properties of the mutant enzymes (R30A, R31A, R221A, R234A, and R257A) tested the authenticity of this putative allosteric site. It should be noted that Arg 221 is conserved throughout evolution, Arg 30 is not well conserved, and Arg 31, Arg 234, and Arg 257 are invariant only in bacterial PRKs (*13*). The resultant mutant enzymes were overexpressed in *E. coli* and isolated, and their kinetics and ability to bind NADH and TNP-ATP were characterized.

NADH and TNP-ATP Binding Studies of Mutant PRKs. The binding constant of NADH and the stoichiometry of binding of the fluorescent ATP analogue TNP-ATP for each mutant enzyme were determined by measuring fluorescence enhancement as a function of ligand concentration (Table 3). It has been shown that TNP-ATP is catalytically active and will only bind to the Mg·ATP site and not the allosteric site (*9*). The stoichiometry of binding for TNP-ATP is essentially unchanged from that of the wild type in all of the arginine mutants. Titration data of this kind have been previously shown to correlate well with stoichiometry data derived using centrifugal gel filtration. It has been estimated that the binding of TNP-ATP must be stronger than 1 μM for successful isolation of a 1:1 binary complex of PRK and TNP-ATP. In contrast to the TNP-ATP result, all of the mutant enzymes with the exception of R221A bind NADH less well than the wild-type enzyme. In fact, there was no detectable fluorescence enhancement for either the R234A or R257A mutant enzyme.

Kinetic Parameters of Allosteric Site Mutants. A kinetic method can be used for evaluating NADH binding to PRK in the quaternary E·Ru5P·ATP·NADH complex that forms under steady-state turnover conditions (*9*). The maximal activity of each of the mutant enzymes was measured with respect to the NADH concentration to determine an upper estimate of the binding constant for the allosteric effector. As can be seen in Table 3, R30A has a K_{aNADH} measured by kinetics that is similar to that of the wild type. Mutant enzyme R234A exhibits a response to high NADH concentrations, whereas R31A and R257A do not respond to NADH addition even at a concentration of 10 mM. In Table 4, the kinetic parameters (the $K_{m,Ru5P}$, the concentration of ATP at half-maximal activity, the Hill coefficient, and the maximum velocity) were determined for each mutant enzyme in the presence of 1 mM NADH. Also included in this table is the extent of stimulation by NADH. This number reflects the maximal activation seen for the wild-type and mutant proteins over the wide range of NADH concentrations employed.

The R221A mutant enzyme is comparable to the wild type with a nearly identical K_d for the NADH binary complex and good NADH activation. In addition, the $K_{m,Ru5P}$ is increased by about 30-fold, a characteristic seen for several active site residues (*19*). The $S_{1/2}$ for ATP binding is higher than that of the wild type by about 10-fold, and V_{max} is about 6-fold lower than that of the wild type. Thus, R221 has more influence on catalysis than allosteric regulation. Allosteric activation by NADH and $K_{m,Ru5P}$ for the R30A mutant enzyme are similar to those of the wild type, even though the K_d for the NADH binary complex is somewhat higher than that of the wild type (Table 3). Thus, R30 does not appear to play a significant role in NADH regulation. Mutant enzymes R31A, R234A, and R257A have relatively unchanged $K_{m,Ru5P}$ constants; however, all three mutants have reduced maximal activity. For R234A and R257A, such a loss in V_{max} correlates well with a weakening or lack of NADH binding. In contrast, R31A retains its ability to bind NADH at the micromolar level.

Kinetics as a Function of ATP in the Presence and Absence of NADH. Plotting the velocity of the reaction as a function of ATP shows that the wild-type enzyme (Figure 3A,B) exhibits hyperbolic kinetics in the absence of NADH and sigmoidal kinetics in the presence of NADH (*9*). The shape of both of these curves for the mutant enzymes R30A and R221A is similar to that of the wild-type enzyme. By contrast, the R234A and R257A mutants both exhibit sigmoidal kinetics versus ATP in either the presence or absence of NADH (Figure 3C,D). However, both the maximal activity and concentration of ATP necessary to obtain half the saturation velocity ($S_{1/2}$) are greatly perturbed from those of the wild-type enzyme. Most strikingly, R31A exhibits nearly identical hyperbolic kinetics in the presence or absence of NADH (Figure 3E). These two activity curves and the wild-type enzyme in the absence of NADH have very similar extrapolated saturation rates and similar $S_{1/2}$ values, suggesting that they share the same allosteric state.

DISCUSSION

The results presented provide evidence that the allosteric binding site for phosphoribulokinase is located between the intersection of three PRK protomers characterized by the high concentration of arginine residues. Structurally, this site does not resemble other known NADH binding sites. Phyloge-

netically, there are three types of arginine residues at this site: Arg 221 which is conserved in both prokaryotic and eukaryotic PRK molecules, Arg 31, Arg 234, and Arg 257 which are conserved in only prokaryotic PRK molecules, and Arg 30 which is not well conserved. Further, Arg 221 is on one subunit, and Arg 234 and Arg 257 are on a second subunit and Arg 30 and Arg 31 on a third subunit whose active site faces the active site of the first subunit. This phylogenetic understanding of these arginine residues can be used to interpret the kinetic data obtained for the mutant enzymes reported here.

Another approach to understanding how PRK is allosterically regulated has recently been described (*20*). A series of chimeric *R. sphaeroides* PRK enzymes have been constructed by expressing spliced together regions of the NADH-sensitive *prkA* and NADH-insensitive *prkB* genes. Analysis of the activities of these chimeras, measured in the presence or absence of NADH, has prompted the conclusion that the N-terminal region of PRK (upstream of Glu 86) is critical to activation by NADH. While Arg 31, which we demonstrate to be crucial to transmission of the allosteric effect, is present in both PRK I and PRK II, the data with chimeric PRKs should be viewed as complementary to our studies. Those observations suggest that other amino acids in this region of PRK I also influence the regulatory linkage that translates binding of activator NADH into an improvement in ATP saturation and enhanced enzyme activity at low levels of this substrate.

It was realized early in the analysis of the kinetic data that despite the potential for stacking with the adenosine moiety of NADH, Arg 221 makes little (or no) contribution to either NADH binding or allosterism. This is reasonable in light of the fact that Arg 221 is conserved in all species of PRK. Further, as noted elsewhere, Arg 221 is located at a three-dimensional position similar to those of catalytically important arginines in other nucleotide monophosphate kinase family enzymes (*13*), and could potentially be involved in Mg·ATP binding. Similarly, Arg 30, which is not well conserved, appears to make only a small contribution to NADH binding and allosterism. Interestingly, the two mutant enzymes (R234A and R257A) that exhibit a significant loss of NADH binding are both found on the same subunit of PRK, while the only arginine mutant (R31A) that exhibits significant binding to NADH and no homotropic cooperativity is on the third subunit.

NADH Binding to the Allosteric Site. Using the position of the AMP-PCP molecule and the known phylogenetic information, it is possible to speculate about which residues other than Arg 31, Arg 234, and Arg 257 may be important for NADH recognition and binding. Since NADH has two ribose rings and two bridging phosphoryls, it makes sense that two orientations of the AMP-PCP molecule should be found. A model may be constructed based upon a combination of both orientations of the AMP-PCP molecule. This model has to be "stretched" so that two phosphoryls can be placed between the two ribose rings. This stretching process may suggest that the two ribose binding sites in the allosteric site move apart from each other when NADH actually binds. The placement of the nicotinamide base to replace one of the adenosine bases is arbitrary, and one of the results of this modeling exercise is shown in Figure 2C. This model suggests that the ribose and nicotinamide rings are located in a cleft that is between the two monomers that make up the "dimer conserved by evolution". Five of the residues, which are in this cleft, are conserved only in bacterial PRKs: Asn 205, Thr 202, and Gln 207 from one protomer and Asp 213 and Ser 215 from the other. It was also possible to build a model that placed the nicotinamide moiety in a cleft that contains Arg 257 and Thr 214. This second model does not use the existing ribose position as a guide, but it does place the nicotinamide ring near a bacterially conserved pocket. Of course, it was also possible to exchange the two bases so that the adenosine ring would be nearby in the lower-temperature factor conformation; however, it was then difficult to find an appropriate placement for the nicotinamide ring. Future studies will attempt to discriminate between these possible nicotinamide binding sites.

Comparison to Other Allosteric Enzymes. Unlike the other structurally well studied allosteric enzymes, glycogen phosphorylase and aspartate transcarbamoylase (ATCase), wild-type phosphoribulokinase exhibits no homotropic cooperativity in the absence of its allosteric activator, NADH. In glycogen phosphorylase, which is a homotetramer, the allosteric AMP binding site is at a dimer interface (*8*), while in ATCase, which is a heterohexamer with three catalytic and three regulatory subunits, the allosteric CTP and ATP binding site is not shared between monomers (*6*, *7*). In both of these enzymes, the T state and the R state differ on the basis of a change in the angular relationship between protomers. The allosteric effector shifts the equilibrium between these two states by binding to one of the states more tightly than the other. In PRK, NADH must be acting in a different manner, as there is no interaction between active sites in its absence. The notion that NADH uses a different set of structural principles to effect homotropic cooperativity is supported by the mutant enzymes R234A and R257A, both of which lack positive charges that interact with the phosphoryls of AMP-PCP and exhibit some homotropic cooperativity in the absence of NADH. Thus, one of the roles for NADH may be to neutralize unfavorable charge−charge interactions which would prevent the enzyme from adopting the R state.

While the R234A and R257A mutant enzymes are defective in NADH binding yet exhibit homotropic cooperativity, the R31A mutant enzyme exhibits the opposite effect on the allosteric behavior of the enzyme. The loss of the arginine residue reduces the level of NADH binding by only 10-fold, yet the transmission of the allosteric signal is entirely blocked. There are examples of mutations in glycogen phosphorylase which lock the enzyme into the T state and increase the affinity for its allosteric regulator, AMP (*21*). However, these mutations are located at the interface near the 2-fold axis of symmetry, a large distance from the allosteric binding site. This type of mutation is substantially different from the Arg 31 mutation, since Arg 31 is located in the allosteric binding site at the interface of three molecules. Functionally, the R31A mutant enzyme acts like the wild-type enzyme in the absence of NADH, since homotropic (ATP) cooperativity is prevented.

NADH Activation versus Allosteric Regulation. Other mutagenesis studies have identified another mutation, R186Q, which exhibits hyperbolic kinetics in the presence of NADH (*19*). However, unlike the R31A mutant enzyme, in the presence of NADH, the R186Q mutant enzyme exhibits a

k_{cat}/K_m ratio which is comparable to that of the wild type. This suggests that the R186Q mutant enzyme is locked in the R state rather than in the T state. It is interesting to note that in the original structure of PRK, a sulfate ion believed to be representative of the phosphoryl of ribulose 5-phosphate is bound by Lys 165, His 69, and Arg 186. The fact that the R186Q mutant appears to be locked into the R state suggests that the conformational changes associated with the R state may effect ribulose 5-phosphate binding and positioning. However, in the absence of NADH, the activity of the R186Q mutant enzyme is reduced 6-fold. This suggests that NADH has two roles in PRK, allowing homotropic cooperativity and enhancing the catalytic rate. As the rate-determining step(s) in PRK catalysis has not been determined, one can only speculate about the basis for the NADH enhancement. However, it is reasonable that the overall catalytic rate is influenced by the large conformational changes that are associated with substrate binding and product release. Thus, bound NADH may increase the rate of the opening and closing of the active site and thus increase the "on" and "off" rates for the substrates and products.

Mechanism for Allosteric Regulation. Since the structure of the R state of this enzyme has not yet been determined, it is only possible to speculate about the nature of the structural changes associated with this transition. In the other allosterically regulated proteins that have been studied in structural detail, including hemoglobin, phosphorylase, and ATCase, it has been shown that the angles in quaternary relationships between protomers change slightly, and these changes are magnified by the large dimensions of a protein relative to an average bond length. The structural changes at the active site are usually quite subtle. If this principle remains true for PRK, then upon binding ATP the quaternary structure must change by a rigid-body rotation of the dimer conserved by evolution relative to the octamer, thus changing the relationship between facing active sites, perhaps allowing residues from one subunit to interact in the other subunit's active site. Further, Arg 31 and NADH must either prevent deleterious interactions from occurring in the R state or make specific contacts in the R state that are not accessible in the T state either with each other or with other residues on neighboring subunits. A second mechanism for homotropic cooperativity can be imagined. ATP binding to one subunit might cause a structural rearrangement of the NADH; this rearrangement would effect the position of Arg 31. Arg 31 is on an α-helix that is directly connected to the P-loop. Thus, a rotation or change of position of this α-helix could directly change the geometry of the active site, and thus increase k_{cat} and decrease K_m for the neighboring subunit. Evidence supporting this second allosteric mechanism comes from the chimeric PRK I and II molecules produced by Tabita et al. (*20*). Two of the amino acid residues that are different at the amino terminus of the two PRK isozymes are found on helix A and pointed in the direction of the active site (residue 23 is a His in PRK I and an Asn in PRK II, while residue 26 is a Asp in PRK I and a Glu in PRK II). However, this sort of allosteric mechanism is unprecedented. Only the three-dimensional structure of the enzyme in the R state will reveal which one of these two hypotheses is correct.

REFERENCES

1. Miziorko, H. M., and Eckstein, F. (1984) *J. Biol. Chem. 259*, 13037.
2. Siebert, K., and Bowien, B. (1984) *Biochim. Biophys. Acta 787*, 208−214.
3. Tabita, F. R. (1980) *J. Bacteriol. 143*, 1275.
4. Buchanan, B. B. (1980) *Annu. Rev. Plant Physiol. 31*, 341.
5. Wedel, N., Soll, J., and Paap, B. K. (1997) *Proc. Natl. Acad. Sci. U.S.A. 94*, 10479.
6. Gouaux, J. E., Stevens, R. C., and Lipscomb, W. N. (1990) *Biochemistry 29*, 7702.
7. Stevens, R. C., Gouaux, J. E., and Lipscomb, W. N. (1990) *Biochemistry 29*, 7691.
8. Barford, D., Hu, S.-H., and Johnson, L. N. (1991) *J. Mol. Biol. 218*, 233.
9. Runquist, J. A., Narasimhan, C., Wolff, C. E., Koteiche, H. A., and Miziorko, H. M. (1996) *Biochemistry 35*, 15049.
10. Bradford, M. (1976) *Anal. Biochem. 72*, 248.
11. Marquardt, D. W. (1963) *J. Appl. Math. 2*, 431.
12. Paulsen, J. M., and Lane, M. D. (1966) *Biochemistry 5*, 2350.
13. Harrison, D. H., Runquist, J. A., Holub, A., and Miziorko, H. M. (1998) *Biochemistry 37*, 5074.
14. Brünger, A. T. (1993) in *X-PLOR Version 3.1 Manual*, Yale Unversity Press, New Haven, CT.
15. Jones, T. A. (1991) *Acta Crystallogr. A47*, 110.
16. Dreusicke, D., Karplus, P. A., and Schultz, G. E. (1988) *J. Mol. Biol. 199*, 359.
17. Muller, C. W., and Schultz, G. E. (1988) *J. Mol. Biol. 202*, 909.
18. Schlauderer, G. J., and Schultz, G. E. (1996) *Protein Sci. 5*, 434.
19. Runquist, J. A., Harrison, D. H. T., and Miziorko, H. M. (1998) *Biochemistry 37*, 1221.
20. Novak, J. S., and Tabita, F. R. (1999) *Arch. Biochem. Biophys. 363*, 273.
21. Buchbinder, J. L., Guinovart, J. J., and Fletterick, R. J. (1995) *Biochemistry 34*, 6423.
22. Laskowski, R. A., MacArthur, M. W., Moss, D. S., and Thornton, J. M. (1993) *J. Appl. Crystallogr. 26*, 283.

BI991033Y